Vacuum 164 (2019) 7–14

Contents lists available at ScienceDirect

Vacuum

journal homepage: www.elsevier.com/locate/vacuum

Effect of Cu additions on mechanical properties of Ni_3Sn_4-based intermetallic compounds: First-principles calculations and nano-indentation measurements

Xiaoyang Bi[a], Xiaowu Hu[a,*], Xiongxin Jiang[a], Qinglin Li[b]

[a] Key Lab for Robot & Welding Automation of Jiangxi Province, Mechanical & Electrical Engineering School, Nanchang University, Nanchang, 330031, China
[b] State Key Laboratory of Advanced Processing and Recycling of Nonferrous Metals, Lanzhou University of Technology, Lanzhou, 730050, China

ARTICLE INFO

Keywords:
Intermetallic compounds
Nano-indentation
First-principles calculations
Mechanical properties

ABSTRACT

The $(Ni,Cu)_3Sn_4$ phase as intermetallic compounds (IMCs) plays an important role in evaluating reliability of solder joints. The first-principles calculations were performed to investigate the phase stability, mechanical properties and electronic structures of Ni_3Sn_4 and $Ni_{2.5}Cu_{0.5}Sn_4$ IMCs. The results shows that the doping of Cu atom not only reduced the phase stability but also weakened the mechanical properties of Ni_3Sn_4 crystal structure. Meanwhile, all studied Ni_3Sn_4-based structures were structural stability. Moreover, the anisotropy of $Ni_{2.5}Cu_{0.5}Sn_4$ (2a site) was strongest while that of $Ni_{2.5}Cu_{0.5}Sn_4$ (4i site) was the weakest. Based on analysis of electronic structures, it indicated that the ionic bonding of Ni−Cu in $Ni_{2.5}Cu_{0.5}Sn_4$ structure was weaker than covalent bonding of nearest-neighbor Ni in Ni_3Sn_4, which led to an energy reduction with the formation of banding states. By means of nano-indentation measurements, the young's modulus and hardness were measured to be 135.3 ± 8.4 GPa and 5.0 ± 0.63 GPa for Ni_3Sn_4 while 126.3 ± 7.6 GPa and 4.7 ± 0.72 GPa for $(Ni,Cu)_3Sn_4$, respectively, which were close to the value of calculated results.

1. Introduction

Soldering is one of the most wildly used technologies in electronic package [1–3]. During the progress of soldering, Sn-based solder will melt and react with pad or plated coating to produce intermetallic compounds (IMCs) which connect solder and substrate. However, substantial thickness of IMCs layer will decrease the reliability of solder joints due to the brittleness of IMCs [4]. In recent years, miniaturization is the main trend in the development of electronic packaging produces [5]. As a result, the mechanical properties of IMCs had developed into a key issue in reliability of solder joints and resulted in a great focuses since volume fraction of IMCs became higher with solder joints becoming smaller [6,7]. In fact, the failure behaviors of solder joints are almost controlled by mechanical properties of IMCs [8]. For example, due to the difference of ductility between IMCs layer and substrate, the stress distribution within solder joints will be changed during reflowing and aging, which harms the reliability of electronic packaging produces.

Ni and Ni-based alloys have became common coating materials in ball grid array (BGA) microelectronic packaging while Sn-based solder was used to reflow with Cu substrate, owing to the fact that Ni layer acted as a barrier layer to impede the diffusion between Sn and Cu element to protect Cu pads. Therefore, the interfacial reactions and IMC growth between Sn-based solders and Ni or Ni-contained substrate have been of interest to many researchers for a long time. Chu et al. [8] researched the interfacial reactions and mechanical reliability of Cu/Sn/Cu and Ni/Sn/Ni sandwich structured solder systems. The results showed that Cu_6Sn_5 was formed in the Cu/Sn/Cu system while Ni_3Sn_4 was formed in the Ni/Sn/Ni system. Additionally, it also reported that the tensile strength of Ni/Sn/Ni samples was weaker than that of Sn/Cu/Sn samples. Related paper [9] noted that the solder joint reliability and elastic stiffness of IMCs are strong couples. Existing experiment data showed that the Yong's module of Ni_3Sn_4 IMC were ranging from 119.4 to 142 GPa [10,11] determined by nano-indentation method. Lee et al. [12] investigated the interfacial reaction of Sn-3.5Ag-0.5Cu (SAC305)/Ni reflowing couples. It reported that $(Ni,Cu)_3Sn_4$ was formed between SAC305 solder and Ni pad, and the thickness of IMC layer increased after aging at 150 °C for 2000 h. It has been also observed by other researches that tracts of Cu atoms were often found in the Ni_3Sn_4 IMC [13,14], in which Ni sublattice were replaced by Cu atoms. Moreover, solid solubility of Cu element was between 5 and 10 at.% in Ni_3Sn_4 phase [15–17]. It is possible that elastic stiffness of

* Corresponding author.
E-mail address: huxiaowu@ncu.edu.cn (X. Hu).

https://doi.org/10.1016/j.vacuum.2019.02.049
Received 9 January 2019; Received in revised form 27 February 2019; Accepted 27 February 2019
Available online 03 March 2019
0042-207X/ © 2019 Elsevier Ltd. All rights reserved.

Ni_3Sn_4 would be altered with the doping of Cu atom. However, most of researches on $(Ni,Cu)_3Sn_4$ IMC were carried out by experimental works and few studies focused on mechanical properties of this IMC. In addition, the influence of the doping of 5–10 at.% Cu atoms on mechanical properties of Ni_3Sn_4 IMC is still unknown whether in laboratory or theoretical studies.

This work is aimed to research the effect of Cu additions on mechanical properties of Ni_3Sn_4 IMC. The mechanical properties of Ni_3Sn_4 and $Ni_{2.5}Cu_{0.5}Sn_4$ phases were predicted by means of first-principles calculations. Besides, the systematically works of the phase stability, electronic properties and elastic constants were carried out to understand the difference between the mechanical properties of Ni_3Sn_4 and $Ni_{2.5}Cu_{0.5}Sn_4$. Moreover, the Ni_3Sn_4 IMCs doped with or without Cu element were produced by reflowing Sn or Sn-0.2Cu solder with Ni substrate. And their Yong's modulus and hardness were measured by using nano-indentation measurements to compare with the predicted results. It is the first systematically work to investigate the mechanical properties of $(Ni,Cu)_3Sn_4$ IMC by combining laboratory and theoretical methods.

2. Experimental and calculation details

2.1. Models and methods

The experimental crystal structure of Ni_3Sn_4 [18] was used as the initial model. As shown in Fig. 1(a), the primitive structure of Ni_3Sn_4 phase was established, in which Ni atoms occupied two different sites: 2a and 4i sites. Different Ni sites were replaced by Cu atoms according to the formula $Ni_{2.5}Cu_{0.5}Sn_4$, in which 7.14 at.% Cu element was doped in the Ni_3Sn_4 phase. The solid solubility of Cu element was within the experimental range of 5–10 at.%. Considering the different sites of Ni atoms, two crystal structures of $Ni_{2.5}Cu_{0.5}Sn_4$ IMC were used in this paper, noted as $Ni_{2.5}Cu_{0.5}Sn_4$ (2a site) and $Ni_{2.5}Cu_{0.5}Sn_4$ (4i site), which were shown in Fig. 1b and c, respectively.

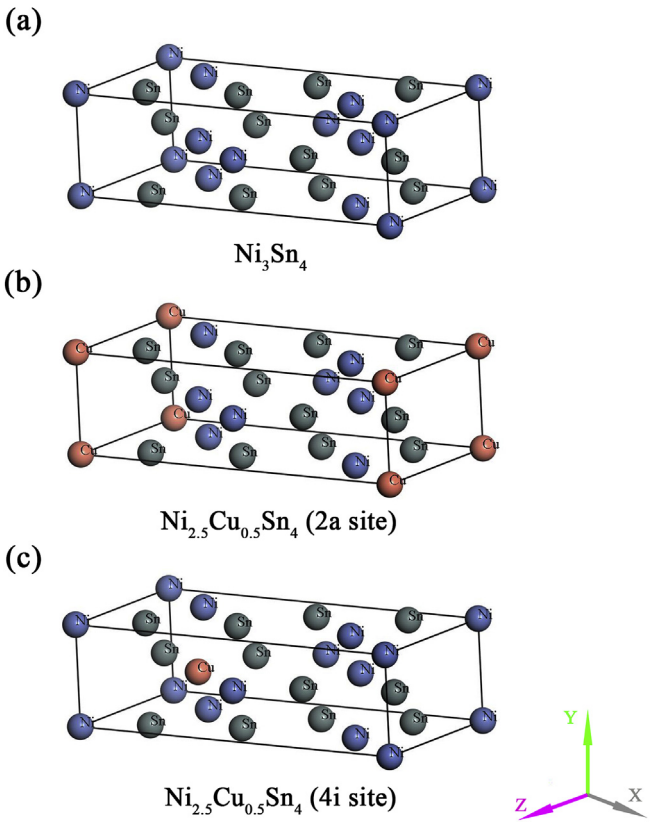

Fig. 1. Crystal structures of (a) Ni3Sn4; (b) Ni2.5Cu0.5Sn4, in which Cu at 2a site; (c) Ni2.5Cu0.5Sn4, in which Cu at 4i site.

In this work, the first-principles calculations were carried out with cambridge serial total energy package (CASTEP) [19]. To ensure the reliability and convergence of calculations, the energy cutoff was set to be 400 eV, and 3 × 9 × 7 meshes of Monkhorst-Pack k-points were adopted to calculate the lattice parameters and elastic constants (C_{ij}) for Ni_3Sn_4 and $Ni_{2.5}Cu_{0.5}Sn_4$ phases. The exchange and correlation functional were treated by the generalized gradient approximation (GGA) for exchange-correlation energy due to Perdew-Burke-Ernzerhof (PBE) [20]. After first-principles calculations, the heat of formation for Ni_3Sn_4 and $Ni_{2.5}Cu_{0.5}Sn_4$ IMCs were calculated by the following formula:

$$\Delta H = E_{total}(Ni_xCu_ySn_z) - [xE_{total}(Ni) + yE_{total}(Cu) + zE_{total}(Sn)] \quad (1)$$

in which $E_{total}(Ni_xCu_ySn_z)$ is the calculated total energy of $Ni_xCu_ySn_z$ at equilibrium lattice constants, $E_{total}(Ni)$, $E_{total}(Cu)$ and $E_{total}(Sn)$ are the energy of the isolated Ni, Cu and Sn atoms, x, y and z are the number of Ni, Cu and Sn atoms in $Ni_xCu_ySn_z$, respectively. Voight-Reuss-Hill (VRH) approximation [21] was used to obtain the bulk and shear modulus of Ni_3Sn_4 and $(Ni,Cu)_3Sn_4$ IMCs. The elastic modulus and Poisson's ratio were calculated by the following equations:

$$B = (B_V + B_R)/2 \quad (2)$$

$$G = (G_V + G_R)/2 \quad (3)$$

$$E = 9BG/(3B + G) \quad (4)$$

$$v = (3B - 2G)/[2(3B + G)] \quad (5)$$

2.2. Experimental works

In the present study, Ni_3Sn_4 IMC was produced by soldering Sn ingot with Ni substrate while $(Ni,Cu)_3Sn_4$ IMC was produced by soldering Sn-0.2Cu alloy with Ni substrate. The raw materials required for this experiment were pure Sn and pure Cu powder (with 99.99% purity). Fig. 2 [14] shows the phase diagrams of Sn—Cu—Ni alloys. According to the weight percentage of Sn-0.2Cu alloy, the ratio of pure Sn powder and pure Cu powder were put into a vacuum induction melting furnace equipped with a pure argon injection system at 500 °C to produce Sn-0.2Cu solder. During melting, the vacuum atmosphere was necessary to obtain a homogeneous Sn-0.2Cu alloy [22,23]. After the materials were completely melted, the liquid melt was isothermally held at 500 °C for about 3 h. After cooling, the original ingot required

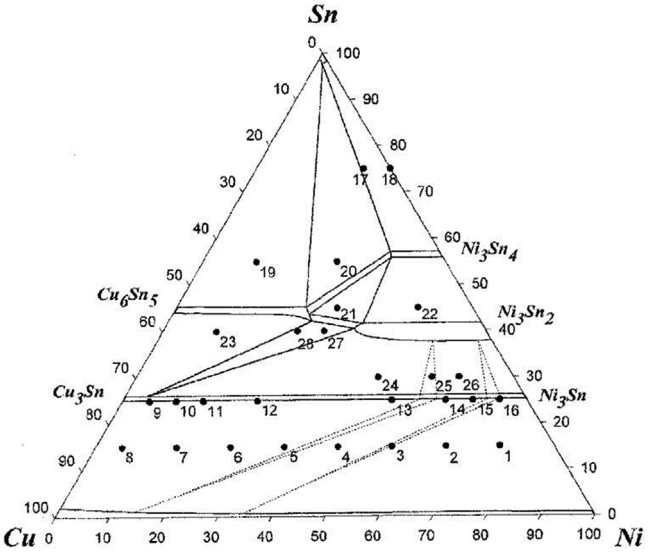

Fig. 2. The phase diagrams of Sn—Cu—Ni alloys [14].

for the experiment was produced.

Ni plates (99.99%) with dimensions 20 × 10 × 2 mm^3 were used as substrates in this work. Before reflowing, the surface of Ni substrates were carefully polished by using 0.1 μm diamond paste, rinsed in water and methanol alcohol and dried. The dip soldering was carried out as following: Firstly, the Sn or Sn-0.2Cu solder was put into a graphite crucible and heated to the temperature of 230 °C. Then, the Ni substrates were carefully immersed in the melted solder for 15 s at the temperature of 230 °C and cooled in air. Finally, the surfaces of the dip soldered joints were cleaned by using methanol alcohol. After dipping soldering, the Sn/Ni and Sn-0.2Cu/Ni couples were aged at 230 °C for 3 h. During the progress of nano-indentation experiments, a thick IMC layer cloud allow nano-indentation to accurately work and easily neglect the influence of the surrounding softer layers. The selected temperature and time of liquid-state aging ensured that Ni_3Sn_4 and $(Ni,Cu)_3Sn_4$ IMCs could accumulate to sufficient thickness, which could improve reliability and accuracy of the experimental results. To analyze the elements of IMCs between Sn or Sn-0.2Cu solder and Ni substrate, the scanning electron microscope (SEM, FEI Quanta200F) and energy dispersive X-ray (EDX) were employed. Before metallographic observations, the reflowed samples were mounted in epoxy and then cross-sectioned in a direction perpendicular to the solder/Ni interface. After that, the specimens were carefully polished and etched with a solution containing 3% HCl, 5% HNO_3 and 92% CH_3OH.

The nano-indentation measurement with a triangular tip was used to measure the Young's modulus and hardness of Ni_3Sn_4 and $(Ni,Cu)_3Sn_4$. In this work, the target depth and strain rate were set to be 1000 nm and 0.2 mN/s. As schematically shown in Fig. 3, nano-indentation tests were carried out within the IMC layer between Sn or Sn-0.2Cu solder and Ni substrate. In order to gain reliable data, ten independent experiments were carried out at individual solder joint.

3. Results and discussion

3.1. Structure optimization

The lattice constants and the heat of formation for Ni_3Sn_4 and $Ni_{2.5}Cu_{0.5}Sn_4$ obtained from experiments and calculations were summarized in Table 1. It could be found that equilibrium lattice parameters obtained in our theoretical works were agreed with available experimental data [18]. The largest deviation was only 1.84% for lattice constant a of Ni_3Sn_4, confirming the accuracy of our calculations. It could be observed that Cu in all phases had little influence on lattice constants, which showed that crystal structures were not changed after the doping of Cu atom into Ni_3Sn_4 phase. To uncover the effect of Cu additions on phase stability of Ni_3Sn_4, the heat of formation (ΔH, meV/atom) at zero temperature and pressure for Ni_3Sn_4 and $Ni_{2.5}Cu_{0.5}Sn_4$ were calculated. A negative value indicates the phase stability with respect to the elemental constituents. Based on our calculations results, all the heat of formation for Ni_3Sn_4-based structures were negative,

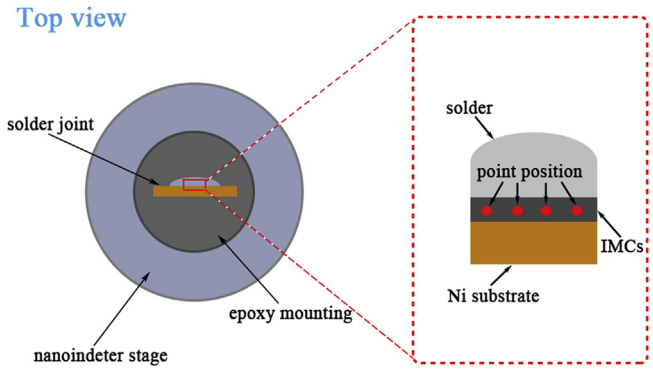

Fig. 3. The locations for nano-indentation tests in tested samples.

Table 1
The lattice constants a, b and c (Å), angle β (°) and the heat of formation (ΔH, meV/atom) of Ni_3Sn_4 and $Ni_{2.5}Cu_{0.5}Sn_4$ obtained from experiments and calculations.

Phases	a	b	c	β	ΔH	Method
Ni_3Sn_4	12.418	4.111	5.315	105.48	−267	Calculation
	12.214[a]	4.060[a]	5.219[a]	105.50[a]	–	Experiment
	12.215[b]	4.060[b]	5.291[b]	105.01[b]	−234[c]	Calculation
$Ni_{2.5}Cu_{0.5}Sn_4$ (2a site)	12.381	4.155	5.330	106.02	−208	Calculation
$Ni_{2.5}Cu_{0.5}Sn_4$ (4i site)	12.426	4.101	5.363	105.69	−193	Calculation

[a] Ref. [18].
[b] GGA-PBE calculated results from Ref. [9].
[c] GGA-PBE calculated results from Ref. [24].

implying the stability at zero temperature and pressure. The heat of formation for Ni_3Sn_4 was −267 meV/atom, which was close to previous calculation result of −234 meV/atom [24]. When Cu atoms were doped in Ni_3Sn_4 structure, the heat of formation increased slightly, with $\Delta H = -208$ meV/atom for $Ni_{2.5}Cu_{0.5}Sn_4$ (2a site) and $\Delta H = -193$ meV/atom for $Ni_{2.5}Cu_{0.5}Sn_4$ (4i site), which meant that the structure of Ni_3Sn_4 was more stable than that of $Ni_{2.5}Cu_{0.5}Sn_4$ IMCs. In other word, the doping of Cu atom weakened the structural stability of Ni_3Sn_4 IMC.

3.2. Mechanical properties

In order to study the effect of Cu additions on mechanical properties of Ni_3Sn_4 phase, the stiffness elastic constants C_{ij} (GPa) and compliance elastic constants S_{ij} (1/GPa) of Ni_3Sn_4-based structures were calculated in this work. The calculated results were listed in Tables 2 and 3. The mechanical stability of crystal structure could be determined by using independent elastic constants. For Ni_3Sn_4-based structures (monoclinic crystal structure), elastic constants should satisfy the following stability criteria [25]:

$$C_{ii} > 0\ (i = 1\text{–}6),\ [C_{11} + C_{22} + C_{33} + 2(C_{12} + C_{13} + C_{23})] > 0$$
$$(C_{33}C_{55} - C_{35}^2) > 0,\ (C_{44}C_{66} - C_{46}^2) > 0,\ (C_{33}C_{22} - 2C_{23}) > 0. \quad (6)$$

From Table 2, for calculated elastic constants C_{ij} of all Ni_3Sn_4-based structures, the corresponding criteria listed in Eq. (6) were easily satisfied. Therefore, the studied Ni_3Sn_4-based structures were mechanical stability at 0 K.

The independent elastic constants could be used to derive theoretical elastic modulus by using VRH approach. The calculated results were shown in Table 4. The Young's modulus of Ni_3Sn_4 phase was 136.78 GPa, which was consistent with the value of 138 GPa determined by nano-indentation measurements [10]. After Cu doping in Ni_3Sn_4 structure, the shear modulus and Young's modulus decreased appreciably, with $G = 48.18$ GPa and $E = 123.99$ GPa for $Ni_{2.5}Cu_{0.5}Sn_4$ (2a site) while $G = 49.62$ GPa and $E = 127.45$ GPa for $Ni_{2.5}Cu_{0.5}Sn_4$ (4i site). It is predicted that the bonding energy of Ni_3Sn_4-based structures was reduced after doping Cu atoms into Ni_3Sn_4 crystal, which led to the decrease of shear modulus and Young's modulus.

According to Pugh's criterion [26], the ratio of B/G is suggested as a condition to distinct brittle and ductile. If the value is higher than 1.75, the material is ductile, otherwise it is brittle. The ratios of B/G for Ni_3Sn_4, $Ni_{2.5}Cu_{0.5}Sn_4$ (2a site) and $Ni_{2.5}Cu_{0.5}Sn_4$ (4i site) were 1.82, 2.01 and 1.95, respectively. Thus all Ni_3Sn_4-based phases could be classified as ductile and Ni_3Sn_4 IMC was the most ductile among all studied structures. In addition, Poisson's ratio (υ) can be also considered as an parameter to represent the ductile or brittle behaviors of materials when υ is higher or lower than 0.25 [27]. According to Poisson's ratio in Table 4, it was expected that all Ni_3Sn_4-based phases were ductile. However, the elastic modulus of IMCs can be predicted by using first-principle calculations, but the actual plastic properties of materials are

Table 2
The calculated elastic constants C_{ij} (GPa) for Ni_3Sn_4 and $Ni_{2.5}Cu_{0.5}Sn_4$.

Phases	C_{11}	C_{12}	C_{13}	C_{22}	C_{23}	C_{33}	C_{44}	C_{55}	C_{66}	C_{15}	C_{25}	C_{35}	C_{46}
Ni_3Sn_4	155.48	70.68	69.34	164.33	68.26	149.86	62.74	59.99	59.95	−21.97	13.99	−8.73	4.90
$Ni_{2.5}Cu_{0.5}Sn_4$ (2a site)	139.83	71.74	65.73	154.57	77.70	154.85	60.10	59.68	56.86	−21.33	13.95	−9.57	6.27
$Ni_{2.5}Cu_{0.5}Sn_4$ (4i site)	146.95	71.79	64.07	176.30	73.29	154.47	57.86	55.11	55.41	−21.79	11.93	−6.18	8.22

also influenced by crystal structures, microstructures, experimental situations and so on [24]. Ghosh researched the ambient temperature isotropic elastic modulus and plastic properties of Ni_3Sn_4 [28]. It is noted that the Ni_3Sn_4 exhibited brittle behaviors under Vickers indentation. But few slip bands were also be observed during the experiment, which implied the limited intrinsic ductility of Ni_3Sn_4 phase. The results showed that the actual plastic properties of materials were rather complex. The Ni_3Sn_4-based phases were classified as ductile by Pugh's criterion in this work, but the actual experimental responses might deviate from this.

It is generally believed that the mechanical responds of materials are largely influenced by evolution and development of microcracks, which is related to elastic anisotropy [29,30]. The elastic anisotropy of a crystal structure was characterized by the universal elastic anisotropy index (A^U) in our work, which could be calculated by the following equation [31]:

$$A^U = 5\frac{G_V}{G_R} + \frac{B_V}{B_R} - 6 \geq 0 \quad (7)$$

in which G_V, G_R, B_V and B_R represented the shear modulus and bulk modulus calculated by Voight and Reuss methods, respectively. When the value of A^U is zero, the crystal structure should be an isotropic structure. A lager value of A^U reveals a stronger anisotropy for a material. The calculated results were listed in Table 5. According to Table 5, all Ni_3Sn_4-based crystal structures were not isotropic structure. Meanwhile, the Cu doping would strengthen the mechanical anisotropy of Ni_3Sn_4 IMC only at a special occupancy site (2a site). In order to further illustrate the mechanical anisotropy of Ni_3Sn_4-based phases, curved surfaces of three-dimensional (3D) were employed in this work. The surface constructions of Young's modulus were defined in the following equation:

$$E^{-1} = l_1^4S_{11} + 2l_1^2l_2^2S_{12} + 2l_1^2l_3^2S_{13} + 2l_1^2l_3^2S_{15} + 2l_2^4S_{22} + 2l_2^2l_3^2S_{23} + 2l_1l_2^2l_3S_{25} + l_3^4S_{33} + 2l_1l_3^3S_{35} + l_2^2l_3^2S_{44} + 2l_1l_2^2l_3S_{46} + l_1^2l_3^2S_{55} + l_1^2l_2^2S_{66}. \quad (8)$$

Here l_1, l_2 and l_3 represented the direction cosines to the x, y and z axes, respectively. S_{ij} were calculated to be elastic constants, as shown in Table 3. The surface construction of an isotropic crystal exhibited to be spherical, while the degree deviating from sphere implied the content of anisotropy. As shown in Fig. 4, the $Ni_{2.5}Cu_{0.5}Sn_4$ (2a site) had the strongest anisotropy while the $Ni_{2.5}Cu_{0.5}Sn_4$ (4i site) had the weakest one. Related paper showed that the elastic modulus of Ni_3Sn_4 IMC varied over a wide range. For example, the reported Young's modulus of Ni_3Sn_4 phase ranged from 119 to 152 GPa determined by nano-indentation measurements [11,12,32] while between 94 and 118 GPa determined by other methods [10,28]. The analysis of elastic anisotropy made it easy to understand the wide range of elastic modulus of Ni_3Sn_4.

Table 4
The calculated bulk modulus (B, GPa), shear modulus (G, GPa), Young's modulus (E, GPa) and Poisson's ratio (υ) for Ni_3Sn_4 and $Ni_{2.5}Cu_{0.5}Sn_4$.

IMCs	B	G	E	υ	B/G
Ni_3Sn_4	98.01	53.96	136.78	0.270	1.82
$Ni_{2.5}Cu_{0.5}Sn_4$ (2a site)	96.88	48.18	123.99	0.287	2.01
$Ni_{2.5}Cu_{0.5}Sn_4$ (4i site)	98.45	49.62	127.45	0.284	1.95

Table 5
The calculated bulk modulus (GPa) and shear modulus (GPa) in VRH approximations and the universal anisotropy index (A^U) for Ni_3Sn_4-based structures.

IMCs	B_V	B_R	G_V	G_R	B_V/B_R	G_V/G_R	A^u
Ni_3Sn_4	98.47	97.56	53.96	49.42	1.001	1.092	0.461
$Ni_{2.5}Cu_{0.5}Sn_4$ (2a site)	97.73	96.03	51.11	45.25	1.018	1.130	0.668
$Ni_{2.5}Cu_{0.5}Sn_4$ (4i site)	99.56	97.33	51.58	47.66	1.013	1.082	0.423

3.3. Electronic structures

To gain deep insight into the nature of the electronic structures, the calculated total density of states (DOS) and partial density of states (PDOS) were shown in Fig. 5, in which Fermi level (E_F) was located at 0 eV and marked by the dashed line. In all cases, it was a remarkable fact that several bands crossed the Fermi level. The electronic property showed that the Ni_3Sn_4 and $Ni_{2.5}Cu_{0.5}Sn_4$ phases were metallic. For Ni_3Sn_4, the sum DOS at energy range from about −12 to −6 eV was main contributed by Sn-*s* state. In the zone from about −6 eV to E_F, the Ni-*d* state was the dominant part of the sum DOS while the Sn-*p* state made significant contributions to DOS. Within the energy range from E_F to −6 eV, the sum DOS was mainly contributed by Ni-*d* and Sn-*p* states. The results were in good agreement with the results of Ghosh [33].

According to a direct comparison between the sum DOS of Cu-doped and Cu-free Ni_3Sn_4-based structures, it was clear to find that the bonding peak between −3 and −1 eV was main difference and the lower bonding peak appeared in both $Ni_{2.5}Cu_{0.5}Sn_4$ (2a site) and $Ni_{2.5}Cu_{0.5}Sn_4$ (4i site) phases. It was contributed to that when Ni sites were replaced by Cu atoms in Ni_3Sn_4 structure, the amplitude of the Ni-*d* state peak was significantly reduced by the reason of the low Ni concentration in $Ni_{2.5}Cu_{0.5}Sn_4$ phases, which weakened the bonding between Ni and Sn atoms. Another difference between the DOS of Ni_3Sn_4 and $Ni_{2.5}Cu_{0.5}Sn_4$ phases was that a second bonding peak appeared at the energy ranging from −5 to −3 eV in Cu-doped structures, which was ascribed to the contribution of Cu-*d* state. However, the peak position of Cu-*d* state corresponded to the saddle-point position of Sn-*p* at the energy level of about −4.5 eV, thus the doped Cu atoms were not able to accommodate the loss of the bonding between Ni and Sn. In a word, the bonding energy of Ni_3Sn_4 was stronger than that of $Ni_{2.5}Cu_{0.5}Sn_4$ crystal structures. As known, lager bonding energy

Table 3
The calculated elastic constants S_{ij} (1/GPa) for Ni_3Sn_4 and $Ni_{2.5}Cu_{0.5}Sn_4$.

Phases	S_{11}	S_{12}	S_{13}	S_{22}	S_{23}	S_{33}	S_{44}	S_{55}	S_{66}	S_{15}	S_{25}	S_{35}	S_{46}
Ni_3Sn_4	0.0098	−0.0034	−0.0027	0.0090	−0.0027	0.0092	0.0160	0.0191	0.0168	0.0030	−0.037	0.0010	−0.0013
$Ni_{2.5}Cu_{0.5}Sn_4$ (2a site)	0.0112	−0.0045	−0.0022	0.0110	−0.0039	0.0094	0.0166	0.0198	0.0178	0.0047	−0.0048	0.0016	−0.0018
$Ni_{2.5}Cu_{0.5}Sn_4$ (4i site)	0.0102	−0.0035	−0.0024	0.0084	−0.0027	0.0088	0.0177	0.0208	0.0184	0.0045	−0.0035	−0.0006	−0.0026

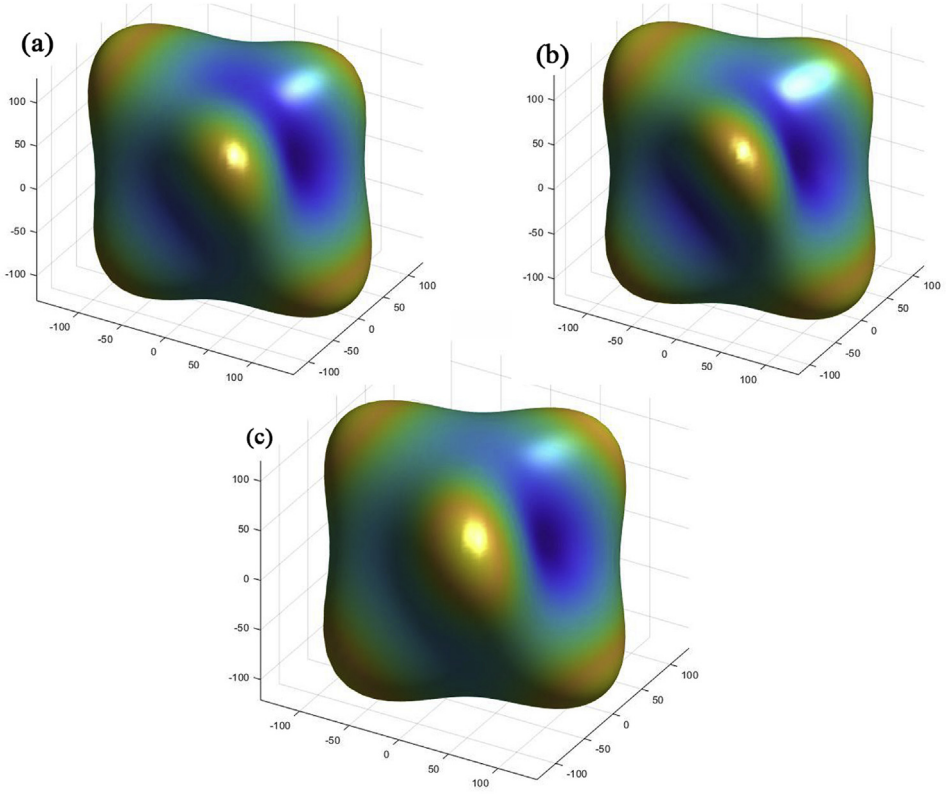

Fig. 4. The surface constructions of Young's modulus for (a) Ni3Sn4, (b) Ni2.5Cu0.5Sn4 (2a site) and (c) Ni2.5Cu0.5Sn4 (4i site).

correspond to a stronger charge interaction [34], and the structural stability will increase. The results might be the reason for the difference of thermodynamic stability and elastic properties between Ni_3Sn_4 and $Ni_{2.5}Cu_{0.5}Sn_4$.

To further understand the bonding mechanisms in Ni_3Sn_4-based structures, the difference charge density maps were illustrated in Fig. 6. The calculated results made it easy to understand the effect of Cu additions on nature of bonding in Ni_3Sn_4-based IMCs. According to Fig. 6(a) and (c), the difference charge density distributions were clearly observed to be positive values at locations of Ni atoms, implying covalent bonding between nearest-neighbor Ni atoms in Ni_3Sn_4 structure. When Cu atoms substituted for Ni atoms at 2a sites in Ni_3Sn_4 crystal structure, the difference charge density maps were altered significantly. As shown in Fig. 6(b), the difference charge density distributions for sites of Cu atoms were calculated to be negative values, which indicated that ionic bonding was formed between nearest-neighbor Ni and Cu atoms. As shown in Fig. 6(d), when Cu atoms occupied 4i sites of Sn atoms in Ni_3Sn_4 crystal structure, the similar effect of additional Cu on nature of bonding in Ni_3Sn_4-based IMCs was discovered, in which the previous Ni—Ni covalent bonding in Cu-free phase changed to be Cu—Ni ionic bonding in Cu-doped phase. As well known, the banding strength of covalent bonding is greater than that of ionic bonding. Therefore, when Cu atoms were doped in Ni_3Sn_4 phase, it indicated that the ionic bonding of the nearest-neighbor Ni and Cu atoms was weaker than the previous Ni—Ni covalent bonding, which led to an energy reduction with the formation of banding states. The results showed that $Ni_{2.5}Cu_{0.5}Sn_4$ IMCs were less resistant to deformation than Ni_3Sn_4, which could explain the mechanism of the decease of stability and modulus of Ni_3Sn_4-based structures.

3.4. Experimental results

The typical cross-section microstructures of solder joints were shown in Fig. 7. In order to confirm the crystal structures of interfacial IMCs between solder and substrate, the EDX and XRD were used in this work. The EDX and XRD results were well presented in Figs. 8 and 9, respectively. For each samples, several analyses were adopted to ensure the reliable of tests. XRD analyses showed that Ni_3Sn_4 structure was identified in Sn/Ni reaction couples. EDX results of the IMC particles showed that Ni_3Sn_4 phase was composed of 41.38 at.% Ni and 58.62 at.% Sn. For the interfacial IMC formed between Sn-0.2Cu solder and Ni substrate, structural analyses showed that the IMC structure was seem to be Ni_3Sn_4 structure. EDX results showed that it was composed of 36.44 at.% Ni, 6.93 at.% Cu and 56.63 at.% Sn, which could be confirmed as $(Ni,Cu)_3Sn_4$ phase. It meant that Cu element showed minimal solubility in Sn-rich phases, which diffused into Ni_3Sn_4 to produce $(Ni,Cu)_3Sn_4$. The results were well agreed with the previous researches [15,16]. It also observed from Fig. 7 that the average thickness of IMC layer accumulated to 34.36 μm for Ni_3Sn_4 and 21.79 μm for $(Ni,Cu)_3Sn_4$ during soldering and liquid-state aging, which allowed easy nano-indentation works while safely neglected the influence of the surrounding softer layers. The location and shape of nanoindents at the solder joint surface were shown and marked by square regions in Fig. 7. It suggested that the target depth and strain rate adopted during nano-indentation experiments were reasonable to measure a single IMC layer and thus the results obtained in this work were reliable and valuable.

In order to discover the effect of additional Cu atoms on the mechanical properties of interfacial IMCs with solder joints, nano-indentation measurements were carried out in this work. Fig. 10 shows the representative indentation loading-depth curves of Ni_3Sn_4 and $(Ni,Cu)_3Sn_4$ IMCs with 0.2 mN/s strain rate at the maximum depth of 1000 nm. It was clearly observe that under the same experimental conditions, the required load for $(Ni,Cu)_3Sn_4$ IMC was lower than Ni_3Sn_4 IMC to reach the maximum depth of 1000 nm. It indicated that the mechanical properties of Ni_3Sn_4 phase were weakened with the doping of Cu atoms, which agreed well with experiment results. For Ni_3Sn_4 IMC, the obtained average values of Young's modulus and hardness were 135.3 ± 8.4 GPa and 5.0 ± 0.63 GPa, respectively,

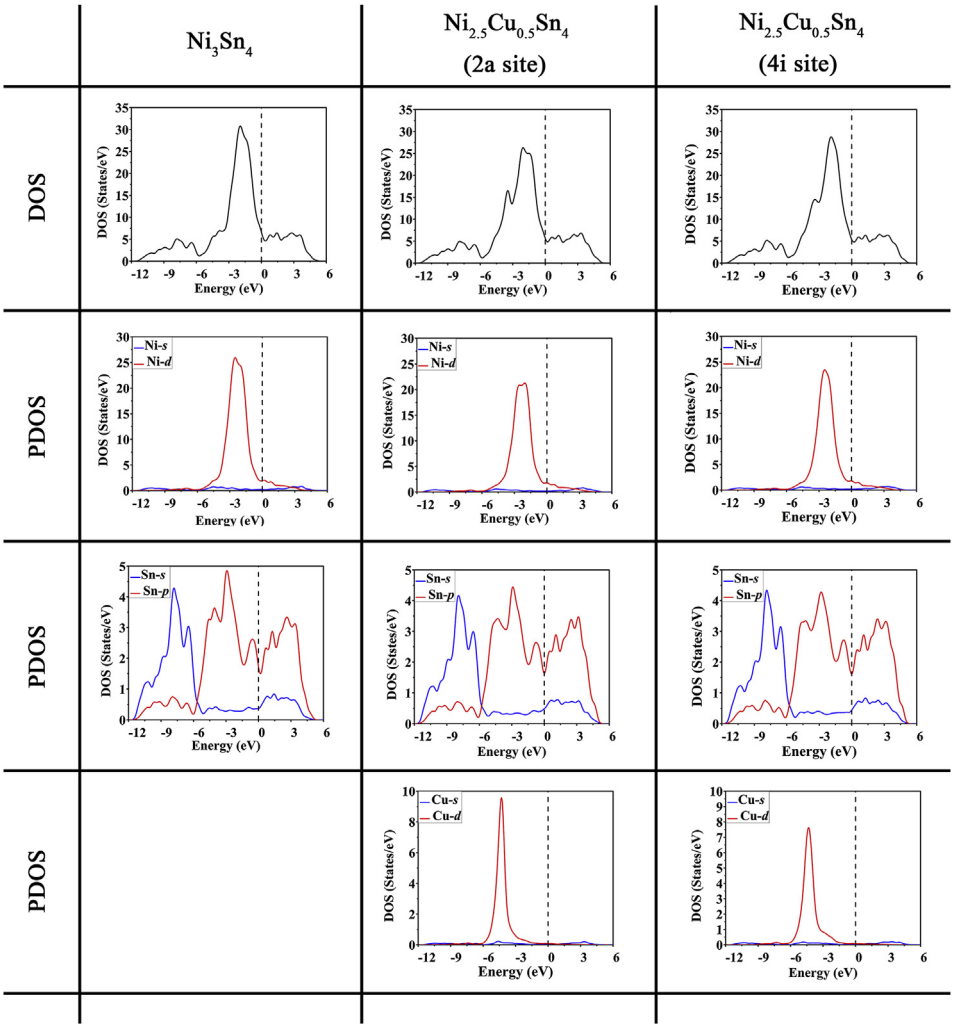

Fig. 5. Density of states (DOS) for Ni3Sn4 and Ni2.5Cu0.5Sn4 with the partial density of states (PDOS) for Ni, Sn and Cu atoms.

which were close to previous results [11,32], in which $E = 134.0$ GPa and $H = 4.8$ GPa. As expected, for $(Ni,Cu)_3Sn_4$, the Young's modulus and hardness were measured to be lower values of 126.3 ± 7.6 GPa and 4.7 ± 0.72 GPa, respectively. It was necessary to point out that Young's modulus of Ni_3Sn_4, $Ni_{2.5}Cu_{0.5}Sn_4$ (2a site) and $Ni_{2.5}Cu_{0.5}Sn_4$ (4i site) were estimated to be 136.78, 123.99 and 127.45 GPa by following first-principles calculations, respectively, which fell nicely within the ranges of the nano-indentation measurement results. Hence, by combining the results of first-principles calculations and experimental works, it demonstrated that the doping of Cu atom was believed to weaken the mechanical properties of Ni_3Sn_4, which was expected to provide valuable information for innovation and usage of solder joints.

4. Conclusions

In this work, the first-principles and nano-indentation measurements were employed to research the effect of additional Cu atoms on the crystal structures and mechanical properties of Ni_3Sn_4 IMC, and the electronic structures of Ni_3Sn_4-based crystals were also discussed. Our systematical works of first-principles calculations predicted that the doping of Cu atom weakened the mechanical properties of Ni_3Sn_4 phase, in which Young's modulus were 136.78 GPa for Ni_3Sn_4 while

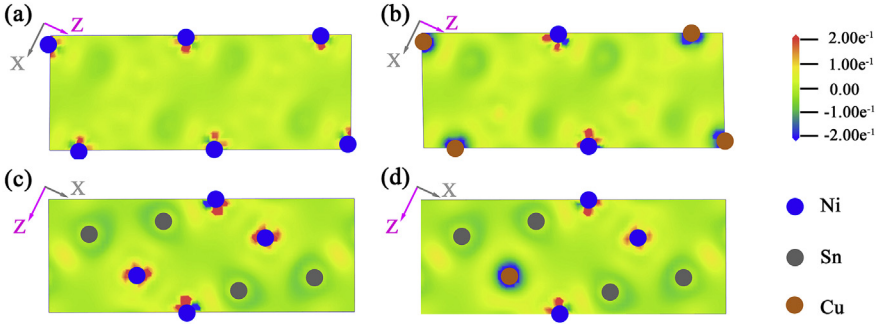

Fig. 6. The difference charge density maps for (a) Ni3Sn4 in (110) plane, (b) Ni2.5Cu0.5Sn4 (2a site) in (110) plane, (c) Ni3Sn4 in (010) plane and (d) Ni2.5Cu0.5Sn4 (4i site) in (010) plane.

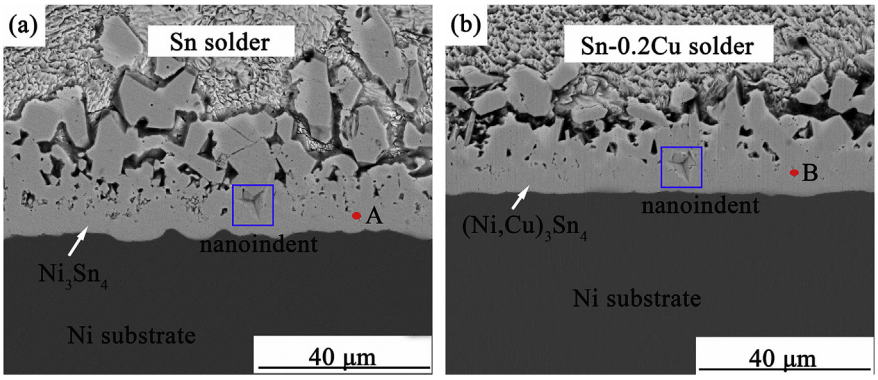

Fig. 7. Cross-sectional microstructure of (a) Sn/Ni reaction couples and (b) Sn-0.2Cu/Ni reaction couples.

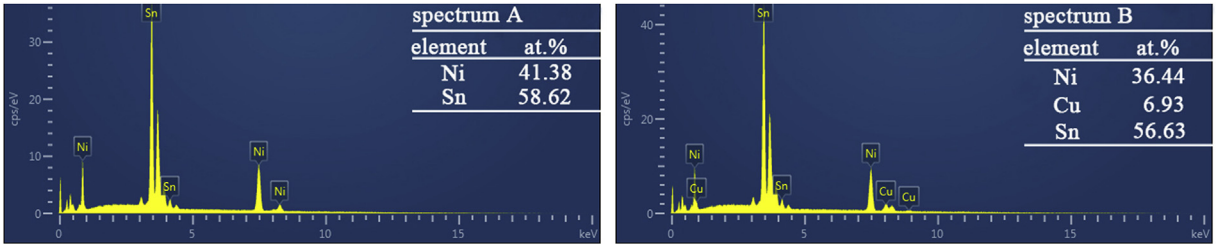

Fig. 8. EDX results of spectrums marked in Fig. 7: spectrum A in Fig. 7(a) and spectrum B in Fig. 7(b).

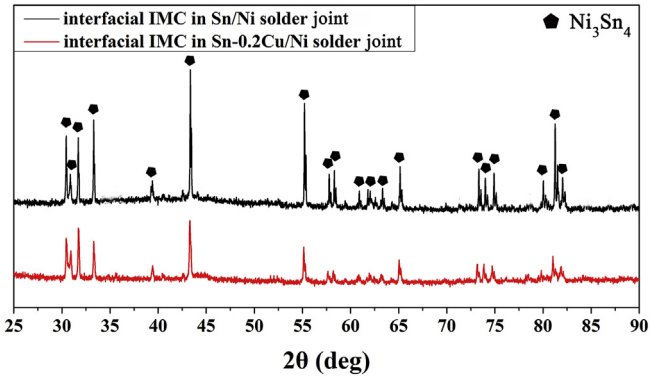

Fig. 9. XRD results for interfacial IMCs of solder joints.

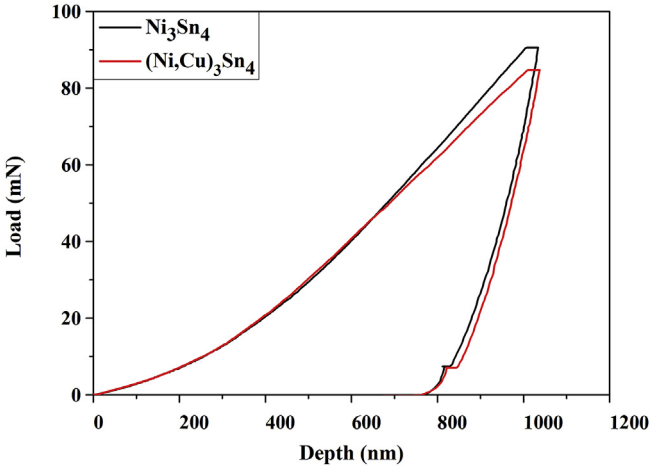

Fig. 10. Indentation loading-depth curves of Ni_3Sn_4 and $(Ni,Cu)_3Sn_4$.

123.99 GPa for $Ni_{2.5}Cu_{0.5}Sn_4$ (2a site) and 127.45 GPa for $Ni_{2.5}Cu_{0.5}Sn_4$ (4i site), respectively. Furthermore, the anisotropy of $Ni_{2.5}Cu_{0.5}Sn_4$ (2a site) was the strongest while that of $Ni_{2.5}Cu_{0.5}Sn_4$ (4i site) was the weakest. Based on the analysis of electronic structures, it indicated that bonding energy between Ni and Sn atoms weakened after the doping of Cu atom, which led to the decrease of Young's modulus. According to the difference charge density maps, the ionic bonding of Ni—Cu in $Ni_{2.5}Cu_{0.5}Sn_4$ structure was weaker than covalent bonding of nearest-neighbor Ni in Ni_3Sn_4. Our nano-indentation measurements showed that the young's modulus and hardness were 135.3 ± 8.4 GPa and 5.0 ± 0.63 GPa for Ni_3Sn_4 while 126.3 ± 7.6 GPa and 4.7 ± 0.72 GPa for $(Ni,Cu)_3Sn_4$, respectively. The calculated Young's modulus fell nicely within the ranges of the experimental results. By combining experimental and calculated results, it was concluded that the doped Cu atoms weakened the mechanical properties of Ni_3Sn_4-based IMCs.

Acknowledgments

This work was supported by the National Natural Science Foundation of China (Nos. 51465039 and 51765040), Natural Science Foundation of Jiangxi Province (20161BAB206122).

References

[1] H. Chen, Y.L. Tsai, Y.T. Chang, A.T. Wu, Effect of massive spalling on mechanical strength of solder joints in Pb-free solder reflowed on Co-based surface finishes, J. Alloy. Comp. 671 (2017) 100–108 https://doi.org/10.1016/j.jallcom.2016.02.027.
[2] C.H. Wang, C.C. Wen, C.Y. Lin, Solid-state interfacial reactions of Sn and Sn-Ag-Cu solders with an electroless Co(P) layer deposited on a Cu substrate, J. Alloy. Comp. 662 (2016) 475–483 https://doi.org/10.1016/j.jallcom.2015.12.060.
[3] J.W. Yoon, C.B. Lee, S.B. Jung, Growth of an intermetallic compound layer with Sn-3.5Ag-5Bi on Cu and Ni-P/Cu during aging treatment, J. Electron. Mater. 32 (2003) 1195–1202 https://doi.org/10.1007/s11664-003-0011-8.
[4] Y. Tang, G.Y. Li, D.Q. Chen, Y.C. Pan, Influence of TiO_2 nanoparticles on IMC growth in Sn-3.0Ag-0.5Cu-*x*TiO2 solder joints during isothermal aging process, J. Mater. Sci. 25 (2014) 981–991 https://doi.org/10.1007/s10854-013-1675-3.
[5] Y. Tang, G.Y. Li, X.Q. Shi, Low-cycle fatigue behavior of 95.8Sn-3.5Ag-0.7Cu solder joints, J. Electron. Mater. 42 (2013) 192–200 https://doi.org/10.1007/s11664-012-2258-4.
[6] Y. Liu, A. Hu, T. Luo, M. Li, Interfacial reaction of Sn-2.0Ag-2.5Zn solder on Cu and Ni-W substrates, J. Mater. Sci. Mater. Electron. 24 (2013) 1037–1044 https://doi.

org/10.1007/s10854-012-0874-7.
[7] S. Chen, W. Zhou, P. Wu, Effect of Zn additions on the mechanical properties of Cu_6Sn_5-based IMCs: theoretical and experimental investigations, J. Electron. Mater. 44 (2015) 3920–3926 https://doi.org/10.1007/s11664-015-3863-9.
[8] K. Chu, Y. Sohn, C. Moon, A comparative study of Cu/Sn/Cu and Ni/Sn/Ni solder joints for low temperature stable transient liquid phase bonding, Scripta Mater. 109 (2015) 113–117 https://doi.org/10.1016/j.scriptamat.2015.07.032.
[9] G. Feng, J. Qu, Elastic modulus of $(Ni,Cu)_3Sn_4$ ternary alloys from first-principles calculations, J. Electron. Mater. 39 (2010) 2429–2434 https://doi.org/10.1007/s11664-010-1338-6.
[10] G.Y. Jang, J.W. Lee, J.G. Duh, The nanoindentation characteristics of Cu_6Sn_5, Cu_3Sn, and Ni_3Sn_4 intermetallic compounds in the solder bump, J. Electron. Mater. 33 (2004) 1103–1110 https://doi.org/10.1007/s11664-004-0111-0.
[11] Z. Chen, M. He, B. Balakrisnan, C.C. Chum, Elasticity modulus, hardness and fracture toughness of Ni_3Sn_4 intermetallic thin films, Mater. Sci. Eng., A 423 (2006) 107–110 https://doi.org/10.1016/j.msea.2005.12.038.
[12] B.S. Lee, Y.H. Ko, J.H. Bang, C.W. Lee, S. Yoo, J.K. Kim, et al., Interfacial reactions and mechanical strength of Sn-3.0Ag-0.5Cu/Ni/Cu and Au-20Sn/Ni/Cu solder joints for power electronics applications, Microelectron. Reliab. 71 (2017) 119–125 https://doi.org/10.1016/j.microrel.2017.03.011.
[13] C.M. Gourlay, K. Nogita, J. Read, A.K. Dahle, Intermetallic formation and fluidity in Sn-rich Sn-Cu-Ni alloys, J. Electron. Mater. 39 (2010) 56–69 https://doi.org/10.1007/s11664-009-0962-5.
[14] C. Lin, S. Chen, C. Wang, Phase equilibria and solidification properties of Sn-Cu-Ni alloys, J. Electron. Mater. 31 (2002) 907–915 https://doi.org/10.1007/s11664-002-0182-8.
[15] V. Vuorinen, H. Yu, T. Laurila, J.K. Kivilahti, Formation of intermetallic compounds between liquid Sn and various $CuNi_x$ metallizations, J. Elevtron. Mater. 37 (2008) 792–805 https://doi.org/10.1007/s11664-008-0411-x.
[16] C.E. Ho, R.Y. Tsai, Y.L. Lin, C.R. Kao, Effect of Cu concentration on the reactions between Sn-Ag-Cu solders and Ni, J. Electron. Mater. 31 (2002) 584–590 https://doi.org/10.1007/s11664-002-0129-0.
[17] C.E. Ho, Y.W. Lin, S.C. Yang, C.R. Kao, D.S. Jiang, Effects of limited Cu supply on soldering reactions between SnAgCu and Ni, J. Electron. Mater. 35 (2006) 1017–1024 https://doi.org/10.1007/BF02692562.
[18] W. Jeitschko, B. Jaberg, Structure refinement of Ni_3Sn_4, Acta Crystallogr. B 38 (1982) 598–600 https://doi.org/10.1107/s056774088200346x.
[19] M.D. Segall, P.L.D. Lindan, M.J. Probert, C.J. Pickard, P.J. Hasnip, S.J. Clark, M.C. Payne, First-principles simulation: ideas, illustrations and the CASTEP code, J. Phys. Condens. Matter 14 (2002) 2717–2744 https://doi.org/10.1088/0953-8984/14/11/301.
[20] J.P. Perdew, K. Burke, M. Ernzerhof, Generalized gradient approximation made simple, Phys. Rev. Lett. 77 (1996) 3865–3868 https://doi.org/10.1103/PhysRevLett.77.3865.
[21] R. Hill, The elastic behaviour of a Crystalline aggregate, Proc. Phys. Soc. 65 (1952) 349–354 https://doi.org/10.1088/0370-1298/65/5/307.
[22] J.X. Chen, X.W. Hu, X.X. Jiang, Interfacial reaction and IMC growth between Sn-37Pb and heterogeneous dual-phase substrate, Vacuum 159 (2019) 112–124 https://doi.org/10.1016/j.vacuum.2018.10.024.
[23] J. Zhao, Q. Yuan, H. Sun, J. Yang, L. Sun, Stability characterization of vacuum encapsulated MEMS resonators with Au-Sn solder bonding, Microsyst. Technol. 24 (2018) 3885–3892 https://doi.org/10.1007/s00542-018-3888-0.
[24] L.H. Li, W.L. Wang, B. Wei, First-principle and molecular dynamics calculations for physical properties of Ni-Sn alloy system, Comput. Mater. Sci. 99 (2015) 274–284 https://doi.org/10.1016/j.commatsci.2014.11.031.
[25] J. Yang, J. Huang, D. Fan, S. Chen, X. Zhao, Structural, mechanical, thermo-physical and electronic properties of η′-$(Cu,Ni)_6Sn_5$ intermetallic compounds: first-principle calculations, J. Mol. Struct. 1112 (2016) 53–62 https://doi.org/10.1016/j.molstruc.2016.01.059.
[26] S.F. Pugh, Relations between the elastic modulus and the plastic properties of polycrystalline pure metals, Mag 45 (1954) 823–843 https://doi.org/10.1080/14786440808520496.
[27] Z.C. Huang, J. Feng, W. Pan, First-principles calculations of mechanical and thermodynamic properties of $YAlO_3$, Comput. Mater. Sci. 50 (2011) 3056–3062 https://doi.org/10.1016/j.commatsci.2011.05.028.
[28] G. Ghosh, Elastic properties, hardness, and indentation fracture toughness of intermetallics relevant to electronic packaging, J. Mater. Res. 19 (2004) 1439–1454 https://doi.org/10.1557/JMR.2004.0193.
[29] Y.Z. Liu, Y.H. Jiang, J. Feng, R. Zhou, Elasticity, electronic properties and hardness of MoC investigated by first principles calculations, Physica B 419 (2013) 45–50 https://doi.org/10.1016/j.physb.2013.03.016.
[30] S.I. Ranganathan, M. Ostoja-Starzewski, Mesoscale conductivity and scaling function in aggregates of cubic, trigonal, hexagonal, and tetragonal crystal, Phys. Rev. B 101 (2008) 214308 https://doi.org/10.1103/PhysRevB.77.214308.
[31] P. Ravindran, L. Fast, P.A. Korzhavyi, B. Johansson, J. Wills, O. Eriksson, Density functional theory for calculation of elastic properties of orthorhombic crystals: application to $TiSi_2$, J. Appl. Phys. 84 (1998) 4891 https://doi.org/10.1063/1.368733.
[32] H.J. Albrecht, A. Juritza, K. Müller, W.H. Müller, J. Sterthaus, J. Villain, A. Vogliano, Interface reactions in microelectronic solder joints and associated intermetallic compounds: an investigation of their mechanical properties using nanoindentation, Proceedings of the 5th Electronics Packaging Technology Conference, Singapore, 2003, pp. 726–731 https://doi.org/10.1109/EPTC.2003.1271613.
[33] G. Ghosh, First-principles calculation of phase stability and cohesive properties of Ni-Sn intermetallics, Metall. Mater. Trans. 40 (2009) 4–23 https://doi.org/10.1007/s11661-008-9682-3.
[34] C.L. Fu, X. Wang, Y.Y. Ye, K.M. Ho, Phase stability, bonding mechanism, and elastic constants of Mo_5Si_3 by first-principles calculation, Intermetallics 7 (1999) 0–184 https://doi.org/10.1016/S0966-9795(98)00018-1.